Press-braked S690 high strength steel equal-leg angle and plain channel section stub columns: Testing, numerical simulation and design

Lulu Zhang [a], Fangying Wang [a], Yating Liang [b], Ou Zhao [*a]

[a] School of Civil and Environmental Engineering, Nanyang Technological University, Singapore

[b] School of Engineering, University of Glasgow, Glasgow, UK

[*] Corresponding author, Email: ou.zhao@ntu.edu.sg

Abstract

This paper reports an experimental and numerical investigation into the cross-section behaviour and compression resistances of press-braked S690 high strength steel angle and channel section stub columns. The experimental study was carried out on four equal-leg angle sections and eight plain channel sections with a range of cross-section sizes (covering both non-slender and slender sections), and included thirty-six material tensile flat and corner coupon tests, initial local geometric imperfection measurements and twenty-four concentrically loaded stub column tests. The experimental study was then supplemented by a numerical modelling programme, where numerical models were firstly developed to simulate the test structural responses and subsequently adopted to derive further numerical data. The experimentally and numerically derived results were utilised to assess the applicability of the Eurocode Class 3 slenderness limits for hot-rolled and welded sections to their cold-formed (press-braked) counterparts. The results of the assessment generally revealed that the Eurocode Class 3 slenderness limits for hot-rolled and welded sections can be safely adopted for the classification of press-braked (cold-formed) S690 high strength steel angle and channel sections subjected to compression. The accuracy of the codified design provisions established in North America, Australia, New Zealand and Europe as well as the direct strength method (DSM) to the design of press-braked S690 high strength steel angle and channel section stub columns was also assessed, based on the test data and numerical results. The North American, Australian and New Zealand standards were found to result in accurate and consistent compression capacity predictions for press-braked S690 high strength steel channel section and non-slender angle section stub columns, but greatly underestimate the compression capacities for those slender angle section stub columns, while the European code and DSM were shown to yield overall precise and consistent design compression capacities.

Keywords: Cross-section behaviour; Design standards; Direct strength method; Equal-leg angle sections; Numerical modelling; Plain channel sections; Stub column tests; S690 high strength steel

1. Introduction

High strength steels, with the nominal yield stresses greater than 460 MPa, possess exceptional strength-to-weight ratios, bringing the possibility of structural components designed with small dimensions and light weights, and are thus being increasingly utilised in the construction of high-rise and long-span structures subjected to heavy vertical loading. Experimental and numerical investigations have been previously performed on various high strength steel structural components of different cross-section shapes, with a brief summary of the experimental studies on stub columns reviewed herein. Nishino et al. [1] and Nishino and Tall [2] reported stub column tests on A514 steel (with the nominal yield stress of 690 MPa) welded box sections to examine their local stability and cross-section resistances in compression. Rasmussen and Hancock [3,4] experimentally studied the local buckling responses and yield slenderness limits of Grade 700 steel (with the nominal yield stress of 690 MPa) stub columns of welded I-, cruciform and box sections. Sun et al. [5] performed a thorough experimental programme on S690 high strength steel welded I-section stub columns, and proposed a new membrane residual stress distribution model and evaluated the accuracy of the established design standards, based on the experimental results. Shi et al. [6,7] reported stub column tests on welded box sections and I-sections made of 460 MPa and 960 MPa high strength steels, and investigated their cross-section compression behaviour and resistances. Jiao and Zhao [8] experimentally studied the initial geometric imperfections, residual stresses and compression resistances of high strength steel (with the nominal yield stress of 1350 MPa) cold-formed circular hollow section stub columns, while the local stability and load-carrying capacities of cold-formed rectangular and square hollow section stub columns made of high strength steels with the nominal yield stresses ranging from 460 MPa to 1100 MPa were experimentally examined by Ma et al. [9] and Wang et al. [10]. The brief review generally indicated that while extensive experimental studies have been conducted on high strength steel doubly symmetric (welded I-, box and cruciform and cold-formed tubular) section stub columns, their non-doubly symmetric counterparts remain unexplored. In comparisons with doubly symmetric tubular and open sections, non-doubly symmetric open sections (e.g., angle and channel sections) are generally much easier to fabricate, but have lower torsional stiffness and are more prone to global instability, particularly torsion-related buckling. Therefore, despite angle and channel section members possessing simple cross-section geometric shapes, their buckling behaviour and design are rather complicated. The findings and design proposals derived from previous studies on doubly symmetric high strength steel sections may not be directly applicable to their non-doubly symmetric angle and channel section counterparts or, at least, require further experimental and numerical verification.

This paper reports a thorough experimental and finite element modelling programme to investigate the cross-section behaviour and compression capacities of press-braked S690 high strength steel equal-leg angle and plain channel section stub columns. The experimental programme was performed on four equal-leg angle sections and eight plain channel sections with cross-section aspect ratios ranging from 1.0 to 3.0, and comprised thirty-six material tensile flat and corner coupon tests, initial local geometric imperfection measurements and twenty-four stub column tests. The finite element modelling programme included a validation study, where numerical models were developed to replicate the structural responses of the tested stub column specimens, and a parametric study, in which the validated numerical models were used to carry out parametric studies to acquire an additional numerical data pool over a wider range of cross-section geometric sizes. The experimentally and numerically derived results were compared with the compression strength predictions by the European code EN 1993-1-12 [11], North American specification AISI S100 [12], Australian/New Zealand standard AS/NZS 4600 [13] and direct strength method [14], enabling the accuracy of each established design approach for press-braked S690 high strength steel equal-leg angle and plain channel section stub columns to be evaluated.

2. Experimental investigation

2.1 General

A comprehensive experimental programme, comprising thirty-six material tensile flat and corner coupon tests, initial local imperfection measurements and twenty-four stub column tests, was firstly conducted to examine the cross-section behaviour and compression capacities of press-braked S690 high strength steel angle and channel section stub columns. Four equal-leg angle sections (A 70×70×5, A 80×80×5, A 90×90×5 and A 100×100×5) and eight plain channel sections (C 60×40×5, C 80×40×5, C 80×50×5, C 80×60×5, C 80×80×5, C 100×40×5, C 100×60×5 and C 120×40×5) were utilised in the present testing programme. The labelling system for angle sections comprises a letter 'A' (representing angle section) and the nominal section sizes (outer leg width b × outer leg width b × wall thickness t – see Fig. 1(a)), while the cross-section designation system for channel sections starts with a letter 'C' (representing channel section), followed by the nominal section sizes (outer web height h × outer flange width b × wall thickness t – see Fig. 1(b)).

2.2 Material testing

Material tensile flat and corner coupon tests were firstly carried out to obtain the stress–strain responses of the considered press-braked S690 equal-leg angle and plain channel sections. One flat coupon and one corner coupon were extracted from each section in the longitudinal direction, with the locations indicated in Fig. 1, while additional sets of flat and corner coupons were also cut from angle sections A 80×80×5 and A 90×90×5 and channel sections C 80×40×5, C 80×60×5, C 80×80×5 and C 100×40×5, for the purpose of conducting repeated tests. The dimensions of all the flat and corner coupons comply with the requirements given in ASTM E8/E8M-15a [15], with the widths and gauge lengths respectively equal to 12.5 mm and 50 mm. An INSTRON 250 kN hydraulic testing machine was adopted to conduct the material tensile coupon tests under displacement control, with the initial loading speed equal to 0.05 mm/min up to the nominal material yield stress of 690 MPa and a higher speed equal to 0.8 mm/min beyond the nominal material yield stress until fracture of the coupons; note that the testing machine is equipped with a series of end clamps, with flat and V-shaped clamps respectively employed for gripping flat and corner coupons. The material tensile coupon test setup is depicted in Fig. 2, in which two strain gauges are affixed to the mid-height of the coupon to measure the tensile strains in the longitudinal direction and an extensometer is mounted onto the necked part of the coupon to record the elongation. Figs 3(a) and 3(b) depict the material stress–strain responses measured from the respective tensile flat and corner coupon tests on the four studied equal-leg angle sections, while the flat and corner material stress–strain curves of the eight examined plain channel sections are respectively displayed in Figs 4(a) and 4(b). The key measured flat and corner material properties for each section are reported in Table 1, in which E is the Young's modulus, f_y is the yield stress, f_u is the ultimate stress, f_u/f_y is the material ultimate-to-yield stress ratio, and ε_u and ε_f are the strains at the ultimate stress and at fracture; note that both the flat and corner portions of the examined press-braked S690 high strength steel angle and channel sections display relatively rounded material responses (see Figs 3 and 4), and the material yield stresses are given as the 0.2% proof stresses [9,10,16,17] in Table 1.

2.3 Measurements on initial local geometric imperfections

Initial local geometric imperfections were introduced into the press-braked S690 high strength steel equal-leg angle and plain channel section stub column specimens during the manufacturing process, and have a detrimental effect on the cross-section compression capacities. The initial local geometric imperfections of each specimen were carefully measured, with the employed test rig [18–21] shown in Fig. 5, where the specimen is placed on a flat milling table and two LVDTs are located at each constituent plate element of the specimen to measure local deviations along two representative longitudinal lines. The initial local geometric imperfections of each plate element were taken as the derivations from a linear regression surface fitted to the data set measured from the two LVDTs [22–25], with the maximum deviations denoted as ω_{f1} and ω_{f2} for flanges of channel section (or legs of angle section) and ω_w for channel web, while the initial local geometric imperfection of the specimen ω_0 is defined as the largest derivation from all the constituent plate elements. Tables 2 and 3 report ω_{f1}, ω_{f2}, ω_w and ω_0 for the press-braked S690 high strength steel equal-leg angle and plain channel section stub column specimens, respectively.

2.4 Stub column tests

For each of the twelve examined press-braked S690 high strength steel equal-leg angle and plain channel sections, two repeated stub column tests were performed to study its cross-section compressive behaviour and capacity. The nominal length of each equal-leg angle section stub column specimen was selected to be three times the outer leg width, while the nominal column length of each channel section specimen was chosen to be three times the mean outer dimension of the web and flange, in conformity with the guidelines set out in Ziemian [26]. Tables 2 and 3 report the measured geometric dimensions of each specimen, where L is the specimen length, b is the outer leg width of angle section or the outer flange width of channel section, h is the outer web height of channel section, t is the wall thickness and r is the internal corner radius. The designation system for stub column specimens begins with the cross-section identifier (A1–A4 representing A 70×70×5, A 80×80×5, A 90×90×5 and A 100×100×5, respectively; C1–C8 representing C 60×40×5, C 80×40×5, C 80×50×5, C 80×60×5, C 80×80×5, C 100×40×5, C 100×60×5 and C 120×40×5, respectively), followed by a letter ‘S’ (indicating stub column), and ends with a number ‘1’ or ‘2’ (for the purpose of distinguishing two repeated tests), e.g., C1-S1 and C1-S2 represent the two plain channel section C 60×40×5 stub column specimens adopted for repeated experiments. An INSTRON

2000 kN hydraulic testing machine equipped with fixed end plates was adopted to perform stub column tests at a uniform speed of 0.1 mm/min. Figs 6(a) and 6(b) display the rigs for equal-leg angle and plain channel section stub column tests, respectively, where two vertical LVDTs are employed to obtain the end shortening of the specimen and a pair of strain gauges are affixed to the mid-height of the specimen to measure the compressive strains in the longitudinal direction. Special anchor devices were utilised at both ends of the specimens to acquire fixed-ended boundary condition and also preclude local failure at the specimen ends. Specifically, the anchor device for angle section stub columns consists of a big base plate (for seating of the specimens) and three small plates with slotted holes (for clamping the ends of the specimens), as shown in Fig. 6(a), while the anchor device for channel section stub columns comprises underpinning bolts (inserted between the two flanges) and G-clamps (clamped onto the outer faces of the flanges), as shown in Fig. 6(b). It is worth noting that the LVDT readings contain both the end shortening of the stub column specimen and the deformation of the end platens of the testing machine. The end-shortening of the stub column specimen was thus obtained through eliminating the deformation of the end platens of the testing machine from the LVDT measurements based on the strain gauge readings [27,28]. This was achieved by assuming that the end platen deformation was proportional to the applied load and shifting the load–end shortening curve derived from the LVDTs such that its initial slope matched that obtained from the strain gauges. The revised (true) load–end shortening responses of the tested press-braked S690 high strength steel equal-leg angle and plain channel section stub column specimens are presented in Figs 7(a) and 7(b), respectively, whilst the key experimental results, including the failure load $N_{u,test}$, end shortening at failure load δ_u and the ratio of $N_{u,test}/(Af_y)$, where A is the gross area of the cross-section, are reported in Table 4. The deformed press-braked S690 high strength steel equal-leg angle and plain channel section stub column specimens are shown in Fig. 8.

3. Numerical modelling investigation

3.1 General

A numerical modelling investigation was presented in this section with the use of the finite element (FE) simulation program ABAQUS [29] to supplement the experimental study. FE models were firstly developed to replicate the structural responses of the tested press-braked S690 high strength steel equal-leg angle and plain channel section stub columns and subsequently employed to carry out parametric studies for the purpose of generating an additional numerical data pool. The derived parametric study results were then adopted, together with the experimentally obtained data, to evaluate the existing design approaches for press-braked S690 high strength steel equal-leg angle and plain channel section stub columns.

3.2 Development of FE models

The 4-noded shell element with reduced integration, S4R, has been extensively adopted for the finite element modelling of thin-walled metallic channel and angle section structural components [20,21,24,30,31], and was therefore also employed herein. The size of the adopted S4R element was selected to be equal to the wall thickness of the modelled section t for both the flat and corner regions of each stub column FE model, based on a prior mesh sensitivity study considering element sizes ranging from $0.2t$ to $3t$. For each press-braked S690 high strength steel angle or channel section, the measured (engineering) flat and corner stress–strain curves were firstly converted into the respective true stress–true plastic strain curves, and then assigned to the flat and corner parts of the corresponding angle or channel section stub column FE model. Note that the corner material properties were only restricted to the curved corners, without extension into the flat portions of the press-braked angle and channel sections, according to the findings of Cruise and Gardner [32]. Previous researchers [33,34] have conducted membrane and bending residual stress measurements on cold-formed steel sections and concluded that the magnitude of the membrane residual stresses was very small compared to that of the bending residual stresses and thus the influence of the membrane residual stresses on the behaviour of cold-formed steel section members was negligible. The bending residual stresses, which were evidenced by the longitudinal curvature of the tensile coupons when they were extracted from the cold-formed steel sections, were approximately reintroduced during tensile testing as the coupons were returned to their straight configuration under the application of tensile loading [33,34]. Therefore, the effect of the bending residual stresses is considered to be inherently presented into the measured material stress–strain responses [33,34]. On this basis, and coupled with the fact that the studied local buckling behaviour is generally insensitive to residual stresses, explicit measurements and modelling of both membrane and bending residual stresses in press-braked (cold-formed) S690 high strength steel angle and channel section stub columns were thus deemed unnecessary.

Suitable boundary conditions were applied to both ends of the stub column FE models to replicate the fixed-ended boundary condition used in the experiments. Specifically, the two end sections were coupled to two concentric reference points, with one fully restrained against translations and rotations and the other one only allowed to translate in the longitudinal direction. Each stub column FE model was then perturbed by its lowest elastic buckling mode shape (i.e. the initial local imperfection distribution pattern was assumed to be of the lowest elastic buckling mode shape [20,21,35,36]); three imperfection levels, including the measured value ω_0 and 1/10 and 1/100 of the wall thickness of the cross-section, were adopted to factor the initial local imperfection distribution shapes, for the purpose of assessing the sensitivity of the press-braked S690 equal-leg angle and plain channel section stub column FE models to the imperfection amplitudes.

3.3 Validation of FE models

Upon development of the stub column finite element models, non-linear static Riks analysis was performed to derive the numerical ultimate loads, load–deformation histories and deformed failure modes, all of which were then compared with the experimental observations, enabling the accuracy of the developed FE models to be evaluated. Table 5 listed the ratios of the numerical to test ultimate loads for the three examined initial local imperfection amplitudes; it was generally found that good agreement was obtained when the imperfection amplitudes of t/10 and the measured imperfection values ω_0 were utilised in the stub column FE models, while the use of the imperfection amplitudes of t/100 into the FE models yielded overestimated ultimate loads. Comparisons between the test and numerical load–end shortening curves for typical press-braked S690 high strength steel equal-leg angle and plain channel section stub column specimens A1-S1 and C3-S1 are shown in Fig. 9, indicating that the full ranges of the experimental load–deformation responses are fully captured by numerical simulation. The failure modes displayed by typical press-braked S690 high strength steel equal-leg angle and plain channel section stub column specimens A1-S1 and C3-S1 are also found to be well replicated by their numerical counterparts, as displayed in Fig. 10. Therefore, it can be concluded that the stub column finite element models developed in Section 3.2 are capable of accurately replicating the stub column tests on press-braked S690 high strength steel equal-leg angle and plain channel sections.

3.4 Parametric studies

The validated finite element models were utilised in this section to carry out parametric studies, to obtain additional numerical data over a wider spectrum of cross-section sizes. Specifically, for the modelled plain channel sections, the outer web heights were fixed at 150 mm, whilst the outer flange widths were chosen to be respectively equal to 50 mm, 60 mm, 75 mm, 100 mm and 150 mm, resulting in five cross-section aspect ratios of 1.0, 1.5, 2.0, 2.5 and 3.0 being examined; for the modelled equal-leg angle sections, four outer leg widths of 70 mm, 90 mm, 110 mm and 130 mm were selected. The wall thicknesses varied from 4 mm to 29 mm, to cover both non-slender and slender equal-leg angle and plain channel sections. It is worth noting that strength enhancements of press-braked sections at the corner zones are related to the cross-section inner corner radius-to-thickness ratios. In order to maintain similar levels of strength enhancements at the corner zones as those of the test press-braked angle and channel sections (all with the inner corner radius-to-thickness ratios equal to 1.5), the inner corner radii of the modelled press-braked angle and channel sections in the parametric studies were fixed to be equal to 1.5 times the wall thicknesses. For each equal-leg angle section stub column FE model, the member length was taken as three times the outer leg width, while for each channel section stub column FE model, the member length was selected to be three times the mean outer dimension of the web and flange. In the present parametric studies, the flat and corner material stress–strain responses of angle section A 70×70×5 were utilised for all the stub column finite element models, and the initial local imperfection amplitudes were taken as 1/10 of the wall thicknesses of the cross-sections. In total, 80 and 60 parametric study results were respectively derived for press-braked S690 high strength steel equal-leg angle and plain channel section stub columns.

4. Evaluation of international design standards

4.1 European code

4.1.1 General

The existing European code EN 1993-1-12 [11] for high strength steels, applicable to steel grades greater than S460 and up to S700, is an extension of the current EN 1993-1-1 [37] for normal strength mild steels with grades less than or equal to S460. Regarding the design of stub columns susceptible to local stability, EN 1993-1-12 [11] follows the same cross-section classification approach and effective width formulations as those adopted in EN 1993-1-1 [37]. Cross-sections are generally categorised into four classes by comparing the $c/t\varepsilon$ ratios of the most slender constituent plate elements against the prescribed slenderness limits, where $\varepsilon=(235/f_y)^{0.5}$ is a material coefficient; note that (i) c is taken as the flat element width excluding the corner radius for webs and flanges of channel sections, but given as the outer element width for legs of angle sections, and (ii) the current EN 1993-1-1 [37] (and also EN 1993-1-12 [11]) only provides slenderness limits for classification of hot-rolled and welded plate elements and cross-sections, with no guidelines on their cold-formed counterparts. Cross-sections categorised as Class 1, 2 and 3 can achieve the yield loads under compression Af_y, while their Class 4 counterparts fail before the material yield stress is attained, limiting the cross-section compression capacities to the effective compression capacities $A_{eff}f_y$, where A_{eff} is the effective area of the cross-section and determined based on the effective width formulations [38]. In the following Section 4.1.2, the suitability of the Eurocode Class 3 slenderness limits for hot-rolled and welded plate elements to their cold-formed (press-braked) counterparts was firstly examined, while assessment of the EC3 cross-section compression resistances was reported in Section 4.1.3.

4.1.2 Class 3 slenderness limits

For all the studied press-braked S690 high strength steel plain channel sections with cross-section aspect ratios falling within the practically used range from 1.0 to 3.0 [39], the outstand flanges are always more critical and slender than the internal webs, i.e. the overall class of a channel section is governed by its flange class. Therefore, only the Class 3 slenderness limit for outstand channel flanges in compression was assessed herein. The experimentally and numerically derived failure loads of press-braked S690 high strength steel plain channel section stub columns, normalised by the corresponding cross-section yield loads, are plotted against the $c/(t\varepsilon)$ ratios of the flanges of the examined channel sections in Fig. 11, together with the Eurocode Class 3 slenderness limit for hot-rolled and welded outstand flanges in compression ($c/(t\varepsilon)$=14). The results of the comparison generally indicated that the Eurocode Class 3 slenderness limit for outstand flanges of hot-rolled and welded channel sections in compression is generally applicable to their cold-formed (press-braked) counterparts.

In comparison with the outstand flanges of channel sections in compression, which benefit from the favourable element interaction provided by the less critical internal webs, the outstand legs of equal-leg angle sections in compression receive no beneficial element interaction from the other outstand legs. Therefore, the current Eurocodes (EN 1993-1-1 [37] and EN 1993-1-12 [11]) utilise a more strict Class 3 slenderness limit for outstand legs of equal-leg angle sections in compression ($c/(t\varepsilon)$=11.5) than that for outstand flanges of channel sections in compression ($c/(t\varepsilon)$=14). A graphic evaluation was carried out on the Class 3 slenderness limit for outstand angle legs in compression, on the basis of the press-braked S690 high strength steel equal-leg angle section stub column test and FE data, as displayed in Fig. 12, indicating that the Eurocode Class 3 slenderness limit for outstand legs of hot-rolled equal-leg angle sections in compression can be safely used for the classification of cold-formed (press-braked) S690 high strength steel equal-leg angle sections.

4.1.3 Cross-section compression capacities

The existing EN 1993-1-12 [11] specifies the use of the yield loads Af_y and effective compression capacities $A_{eff}f_y$ as the design cross-section resistances for non-slender (Class 1, 2 and 3) and slender (Class 4) sections in compression. The effective area of a slender section is equal to the sum of the effective areas of the constituent plate elements, while the effective area of each plate element is given as the product of the effective plate element width and the wall thickness. EN 1993-1-12 [11] adopts different effective width formulations for outstand and internal plate elements, as given in Eqs (1) and (2), respectively, where c_{eff} is the effective plate element width, $\bar{\lambda}_p$ is the local slenderness of the plate element and derived from Eq. (3), where f_{cr} is the elastic local buckling stress of the plate element, and k_σ is the bucking factor and equal to 0.43 and 4.0 for uniformly compressed outstand and internal plate elements, respectively, and ψ is the end stress ratio of the plate element and equal to unity for uniform compressive stress distribution.

$$c_{eff} = \left(\frac{1}{\bar{\lambda}_p} - \frac{0.188}{\bar{\lambda}_p^{\,2}} \right) c \le c \quad \text{for } \bar{\lambda}_p \ge 0.748 \tag{1}$$

$$c_{eff} = \left(\frac{1}{\bar{\lambda}_p} - \frac{0.055(3+\psi)}{\bar{\lambda}_p^{\,2}} \right) c \le c \quad \text{for } \bar{\lambda}_p \ge 0.673 \tag{2}$$

$$\bar{\lambda}_p = \sqrt{\frac{f_y}{f_{cr}}} = \frac{c/t}{28.4\varepsilon\sqrt{k_\sigma}} \tag{3}$$

The EC3 design cross-section compression capacities for press-braked S690 high strength steel equal-leg angle and plain channel section stub columns were evaluated through comparisons against the test and FE failure loads. As reported in Table 6, the mean test and numerical to EC3 predicted failure load ratios $N_u/N_{u,EC3}$, are equal to 1.07 and 1.32 for press-braked S690 high strength steel non-slender and slender equal-leg angle section stub columns, respectively, with the coefficient of variations (COVs) of 0.03 and 0.05, while the mean ratios of $N_u/N_{u,EC3}$ are respectively equal to 1.05 and 1.06, with the corresponding COVs of 0.04 and 0.07, for their non-slender and slender plain channel section counterparts, revealing a good level of accuracy and consistency of the EC3 design rules. This can also be seen from Fig. 13, where the test and numerical to EC3 predicted failure load ratios $N_u/N_{u,EC3}$ are plotted against the local slendernesses $\bar{\lambda}_p$ of the outstand flanges (or legs) of the examined plain channel (or equal-leg angle) sections. Moreover, it is worth noting that the EC3 effective width formulations generally lead to more conservative compression resistance predictions for slender angle sections (with the mean $N_u/N_{u,EC3}$ ratio of 1.32) than for slender channel sections (with the mean $N_u/N_{u,EC3}$ ratio of 1.06). It may be primarily due to the fact that the EC3 effective width reduction factors for angle sections were conservatively calculated based on the full plate element widths including the corner radii, thus leading to lower effective element widths and effective compression resistances, in comparisons with those for channel sections, which were all determined based on the flat plate element widths excluding the corner radii.

4.2 North American Specification and Australian/New Zealand Standard

The North American specification AISI S100 [12] and Australian/New Zealand standard AS/NZS 4600 [13] were established for steels with grades up to S690, and provide the same provisions regarding the design of compression members. For concentrically loaded plain channel section columns (regardless of member lengths), the nominal axial strengths are determined from Eq. (4), where A_{eff} is the effective cross-section area at the design failure stress f_n and determined on the basis of the effective width formula given by Eq. (5), in which c is taken as the flat element width excluding the corner radius and $\lambda = \sqrt{f_n / f_{cr}}$; note that AISI S100 [12] and AS/NZS 4600 [13] use the same effective width formula for both the outstand and internal plate elements in compression, and f_n is the design failure stress, taking into account the interaction of global buckling with local buckling, and derived from Eq. (6), where $\lambda_c = \sqrt{f_y / f_{cre}}$, in which f_{cre} is the least of the member elastic torsional, flexural-torsional and flexural buckling stresses; note that for channel section stub columns, the design failure stress f_n approximates to the material yield stress f_y. With regards to concentrically loaded equal-leg angle section columns (regardless of member lengths), both of the two standards specify that they should always be designed as eccentrically loaded beam-columns with the eccentricities with respect to the cross-section minor principal axes equal to L/1000 [12,13], on the basis of the interaction formula given by Eq. (7), where N_{an} is the design compression strength, N_{nl} is the nominal axial strength and calculated from Eqs (4)–(6), in which f_n shall be determined based only on flexural buckling for non-slender angle sections (i.e. f_{cre} is equal to the member elastic flexural buckling stress in calculating λ_c), but derived according to the most critical member (flexural-torsional) buckling mode for slender angle sections (i.e. f_{cre} is equal to the member elastic flexural-torsional buckling stress in calculating λ_c); note that for non-slender angle section stub columns, the design failure stress f_n approximates to the material yield stress f_y, while for slender angle section stub columns, the design failure stress f_n can be much less than the material yield stress f_y; M_{nl} is the flexure strength, respectively taken as the elastic and effective moment capacities for non-slender and slender sections.

$$N_{nl} = A_{eff} f_n \tag{4}$$

$$c_{eff} = \left(\frac{1}{\lambda} - \frac{0.22}{\lambda^2}\right) c \le c \quad \text{for } \lambda \ge 0.673 \tag{5}$$

$$f_n = \begin{cases} \left(0.658^{\lambda_c^2}\right) f_y & \text{for } \lambda_c \le 1.5 \\ \left(\dfrac{0.877}{\lambda_c^2}\right) f_y & \text{for } \lambda_c > 1.5 \end{cases} \tag{6}$$

$$\frac{N_{an}}{N_{nl}} + \frac{N_{an} L/1000}{M_{nl}} = 1 \tag{7}$$

Quantitative and graphic comparisons of the predicted compression strengths by AISI S100 [12] and AS/NZS 4600 [13] with the test and numerical results were conducted and presented in Table 6 and Fig. 14, respectively. The mean test and FE to predicted strength ratios $N_u/N_{u,AISI}$ (or $N_u/N_{u,AS/NZS}$) are equal to 1.05 and 1.11, with the COVs of 0.04 and 0.07, for press-braked S690 high strength steel non-slender and slender plain channel section stub columns, respectively, while the $N_u/N_{u,AISI}$ (or $N_u/N_{u,AS/NZS}$) ratios are equal to 1.09 and 1.88, with the corresponding COVs of 0.05 and 0.58, for their non-slender and slender equal-leg angle section counterparts. The comparison results generally revealed that the American and Australian/New Zealand standards result in accurate and consistent compression strengths for press-braked S690 high strength steel plain channel section stub columns and non-slender equal-leg angle section stub columns, but rather conservative and scattered design strengths for those slender equal-leg angle section stub columns.

The undue conservatism and scatter of the AISI (or AS/NZS) compression strengths for press-braked S690 high strength steel slender equal-leg angle section stub columns can be principally attributed to the unrealistic small design failure stress calculated from flexural-torsional buckling (for example, the calculated design failure stress for the angle section stub column specimen A4-S1 is only equal to 26% of the material yield stress). It is therefore proposed that the design failure stress be taken as the material yield stress for slender angle section stub columns. On this basis, the AISI (or AS/NZS) compression strengths for press-braked S690 high strength steel slender equal-leg angle section stub columns were calculated, with the mean $N_u/N_{u,AISI,r}$ (or $N_u/N_{u,AS/NZS,r}$) ratio of 1.13 and the corresponding COV of 0.04 (see Table 6), revealing the design accuracy and consistency of AISI S100 [12] and AS/NZS 4600 [13] has been dramatically improved, as can also be seen from Fig. 15.

5. Direct strength method

The direct strength method (DSM) was proposed by Schafer and Peköz [14], aiming at overcoming the cumbersome nature of the effective width approach for the design of cold-formed steel slender section structural components of complex geometries. The key characteristics of the DSM lies in the adoption of a 'strength curve', which allows for direct attainment of the local buckling strength of a slender section based on the cross-section slenderness. The DSM design formulation is given by Eq. (8), in which $\lambda_l = \sqrt{f_y / f_{crl}}$ is the cross-section slenderness, where f_{crl} is the cross-section elastic local buckling stress and can be derived from the finite strip software CUFSM [40]. The DSM has been incorporated into the North American specification AISI S100 [12] and applicable to cold-formed steel lipped channel, Z-, rack and hat sections with the material yield stresses less than 95 ksi (655 MPa). Therefore, the studied S690 high strength steel equal-leg angle and plain channel sections are out of the application scope of the DSM.

$$N_{u,DSM} = \begin{cases} Af_y & \text{for } \lambda_l \leq 0.776 \\ (1-\dfrac{0.15}{\lambda_l^{0.8}})\dfrac{1}{\lambda_l^{0.8}}Af_y & \text{for } \lambda_l > 0.776 \end{cases} \quad (8)$$

The applicability of the DSM [14] to the design of press-braked S690 high strength steel equal-leg angle and plain channel section stub columns was evaluated through comparing the DSM strength predictions with the test and FE failure loads. As presented in Table 6, the mean experimental and FE to DSM predicted compression strength ratios $N_u/N_{u,DSM}$ are both equal to 1.05 for S690 high strength steel non-slender equal-leg angle and plain channel section stub columns, with the corresponding COVs of 0.05 and 0.04, respectively, while the ratios of $N_u/N_{u,DSM}$ are equal to 1.02 and 1.04, with the COVs of 0.02 and 0.07, for slender angle and channel section stub columns, respectively. A graphic evaluation of the DSM strength predictions against the experimental and FE results is also shown in Fig. 16. The quantitative and graphic assessment results generally indicated that the DSM yields more precise and consistent compression strength predictions than the established design codes, especially for those slender angle and channel section stub columns.

Evaluation of the established design codes and the direct strength method (DSM) [14] was also performed based on the test data only, with the test to predicted failure load ratios $N_{u,test}/N_{u,pred}$ for each design approach listed in Table 4. Note that each considered design approach leads to the same classification of the tested equal-leg and plain channel sections; specifically, the four tested equal-leg angle sections are all defined as slender sections, while the tested plain channel sections C 80×50×5, C 80×60×5, C 80×80×5, and C 100×60×5 are classified as slender sections, with the other four defined as non-slender sections. The DSM was shown to yield the highest level of design accuracy and consistency among the considered approaches, with accurate and consistent compression capacity predictions for all the tested press-braked S690 high strength steel equal-leg angle and plain channel section stub columns, followed by the European code EN 1993-1-12 [11]. The North American specification AISI S100 [12] and Australian/New Zealand standard AS/NZS 4600 [13] leads to accurate and consistent compression capacity predictions for the tested press-braked S690 high strength steel plain channel section stub columns, but rather conservative and scattered predicted capacities for those slender equal-leg angle section stub columns. The revised AISI (or AS/NZS) design rules were shown to lead to accurate and consistent compression capacity predictions for all the tested S690 high strength steel angle and channel section stub columns.

6. Conclusions

A systematic experimental and numerical study has been performed to examine the cross-section stability and resistances of press-braked S690 high strength steel equal-leg angle and plain channel section stub columns in compression. The experimental study included thirty-six material tensile flat and corner coupon tests, initial local geometric imperfection measurements and twenty-four stub column tests, whilst the FE investigation comprised a simulation study to replicate the structural responses of the tested stub columns and a parametric study to acquire additional numerical data over a wider range of cross-section dimensions. The test and numerical results were firstly employed to assess the suitability of the Eurocode Class 3 slenderness limits for welded and hot-rolled high strength steel outstand plate elements to their cold-formed (press-braked) counterparts, indicating that the Eurocode Class 3 slenderness limits can be accurately and safely adopted for classifying press-braked S690 high strength steel angle and channel sections. The accuracy of the cross-section compression capacities predicted from the existing EN 1993-1-12 [11], AISI S100 [12], AS/NZS 4600 [13] and direct strength method [14] was also assessed, on the basis of the test and numerical results. The results of the evaluation generally revealed that (i) the DSM [14] and EN 1993-1-12 [11] result in accurate and consistent compression capacity predictions for press-braked S690 high strength steel equal-leg angle and plain channel section stub columns, (ii) AISI S100 [12] and AS/NZS 4600 [13] lead to a good level of accuracy and consistency for the design of press-braked S690 high strength steel plain channel section stub columns and non-slender equal-leg angle section stub columns, but yield unduly conservative and scattered capacity predictions for their slender equal-leg angle section stub column counterparts, owing to the consideration of torsional buckling in the design, and (iii) revised AISI and AS/NZS design rules were proposed through only accounting for local buckling in the design of slender angle section stub columns, leading to significantly more precise and consistent design compression capacities.

Acknowledgements

The authors would like to thank SSAB Swedish Steel Pte Ltd, Singapore for the assistance in fabricating press-braked S690 high strength steel equal-leg angle sections and plain channel sections. NTU Research Scholarship is also acknowledged.

References

[1] Nishino F, Ueda Y, Tall L. Experimental investigation of the buckling of plates with residual stresses. Fritz engineering laboratory report. Bethlehem, Pennsylvania: Lehigh University; 1966.

[2] Nishino F, Tall L. Experimental investigation of the strength of T-1 steel columns. Fritz Engineering Laboratory, Department of Civil Engineering, Lehigh University, 1970.

[3] Rasmussen K J R, Hancock G J. Plate slenderness limits for high strength steel sections. Journal of Constructional Steel Research, 1992, 23(1): 73-96.

[4] Rasmussen K J R, Hancock G J. Tests of high strength steel columns. Journal of Constructional Steel Research, 1995, 34(1): 27-52.

[5] Sun Y, Liang Y, Zhao O. Testing, numerical modelling and design of S690 high strength steel welded I-section stub columns. Journal of Constructional Steel Research, 2019, 159: 521-533.

[6] Shi G, Zhou W, Bai Y, Lin C. Local buckling of 460 MPa high strength steel welded section stub columns under axial compression. Journal of Constructional Steel Research, 2014, 100: 60-70.

[7] Shi G, Zhou W, Lin C. Experimental investigation on the local buckling behavior of 960 MPa high strength steel welded section stub columns. Advances in Structural Engineering, 2015, 18(3): 423-437.

[8] Jiao H, Zhao X L. Imperfection, residual stress and yield slenderness limit of very high strength (VHS) circular steel tubes. Journal of Constructional Steel Research, 2003, 59(2): 233-249.

[9] Ma J L, Chan T M, Young B. Experimental investigation on stub-column behavior of cold-formed high-strength steel tubular sections. Journal of Structural Engineering (ASCE), 2015, 142(5): 04015174.

[10] Wang J, Afshan S, Schillo N, Theofanous M, Feldmann M, Gardner L. Material properties and compressive local buckling response of high strength steel square and rectangular hollow sections. Engineering Structures, 2017, 130: 297-315.

[11] EN 1993-1-12. Eurocode 3: Design of steel structures – Part 1–12: Additional rules for the extension of EN 1993 up to steel grades S 700. Brussels (Belgium): CEN; 2007.

[12] AISI S100. North American specification for the design of cold-formed steel structural members. American Iron and Steel Institute; 2016.

[13] AS/NZS 4600. Cold-formed steel structures. Sydney: AS/NZS 4600:2005; 2005.

[14] Schafer B W. The direct strength method of cold-formed steel member design. Journal of Constructional Steel Research, 2008, 64(7-8): 766-778.

[15] American Society for Testing and Materials (ASTM). Standard test methods for tension testing of metallic materials. E8/E8M-15a. West Conshohocken, PA., USA: ASTM International; 2015.

[16] Fang H, Chan T M, Young B. Material properties and residual stresses of octagonal high strength steel hollow sections. Journal of Constructional Steel Research, 2018, 148: 479-490.

[17] Li H T, Young B. Tests of cold-formed high strength steel tubular sections undergoing web crippling. Engineering Structures, 2017, 141: 571-583.

[18] Schafer B, Peköz T. Computational modeling of cold-formed steel: characterizing geometric imperfections and residual stresses. Journal of Constructional Steel Research, 1998;47(3):193–210.

[19] Landesmann A, Camotim D, Dinis P B, et al. Short-to-intermediate slender pin-ended cold-formed steel equal-leg angle columns: Experimental investigation, numerical simulations and DSM design. Engineering Structures, 2017, 132: 471-493.

[20] Liang Y, Jeyapragasam V V K, Zhang L, Zhao O. Flexural-torsional buckling behaviour of fixed-ended hot-rolled austenitic stainless steel equal-leg angle section columns. Journal of Constructional Steel Research, 2019, 154: 43-54.

[21] Zhang L, Tan K H, Zhao O. Experimental and numerical studies of fixed-ended cold-formed stainless steel equal-leg angle section columns. Engineering Structures, 2019, 184: 134-144.

[22] Zhao O, Rossi B, Gardner L, Young B. Behaviour of structural stainless steel cross-sections under combined loading–Part I: Experimental study. Engineering Structures, 2015, 89: 236-246.

[23] Zhao O, Rossi B, Gardner L, Young B. Experimental and numerical studies of ferritic stainless steel tubular cross sections under combined compression and bending. Journal of Structural Engineering (ASCE), 2015, 142(2): 04015110.

[24] Liang Y, Zhao O, Long Y, Gardner L. Stainless steel channel sections under combined compression and minor axis bending–Part 1: Experimental study and numerical modelling. Journal of Constructional Steel Research, 2019, 152: 154-161.

[25] Su M N, Young B, Gardner L. Testing and design of aluminum alloy cross sections in compression. Journal of Structural Engineering (ASCE), 2014, 140(9): 04014047.

[26] Ziemian RD. Guide to stability design criteria for metal structures. 6th ed. John Wiley & Sons; 2010.

[27] Centre for Advanced Structural Engineering. Compression tests of stainless steel tubular columns. Investigation report S770. University of Sydney; 1990.

[28] Gardner L, Nethercot D A. Experiments on stainless steel hollow sections—Part 1: Material and cross-sectional behaviour. Journal of Constructional Steel Research, 2004, 60(9): 1291-1318.

[29] Hibbitt, Karlsson & Sorensen, Inc. ABAQUS. ABAQUS/Standard user's manual volumes I-III and ABAQUS CAE manual. Version 6.12. Pawtucket (USA); 2012.

[30] Dinis P B, Camotim D, Silvestre N. On the mechanics of thin-walled angle column instability. Thin-Walled Structures, 2012, 52: 80-89.

[31] Dinis P B, Camotim D. A novel DSM-based approach for the rational design of fixed-ended and pin-ended short-to-intermediate thin-walled angle columns. Thin-Walled Structures, 2015, 87: 158-182.

[32] Cruise R B, Gardner L. Strength enhancements induced during cold forming of stainless steel sections. Journal of constructional steel research, 2008, 64(11): 1310-1316.

[33] Rasmussen K J R, Hancock G J. Design of cold-formed stainless steel tubular members. I: Columns. Journal of Structural Engineering, 1993, 119(8): 2349-2367.

[34] Ma J L, Chan T M, Young B. Material properties and residual stresses of cold-formed high strength steel hollow sections. Journal of Constructional Steel Research, 2015, 109: 152-165.

[35] Chen M T, Young B. Material properties and structural behavior of cold-formed steel elliptical hollow section stub columns. Thin-Walled Structures, 2019, 134: 111-126.

[36] Chen M T, Young B. Cross-sectional behavior of cold-formed steel semi-oval hollow sections. Engineering Structures, 2018, 177: 318-330.

[37] EN 1993-1-1. Eurocode 3: Design of steel structures – Part 1–1: General rules and rules for buildings. Brussels (Belgium): CEN; 2005.

[38] EN 1993-1-5. Eurocode 3: Design of steel structures – Part 1–5: Plated structural elements. Brussels: European Committee for Standardization (CEN); 2015.

[39] SSAB. Data sheet 2045 Strenx® Section 700. 2017. https://www.ssab.com/api/sitecore/Datasheet/GetDocument?productId=41C95467C75041D6AE0571B649DA878B&language=en

[40] Schafer BW, Ádány S. Buckling analysis of cold-formed steel members using CUFSM: conventional and constrained finite strip methods. Proceedings of the Eighteenth International Speciality Conference on Cold-formed Steel Structures, Orlando, USA; 2006.

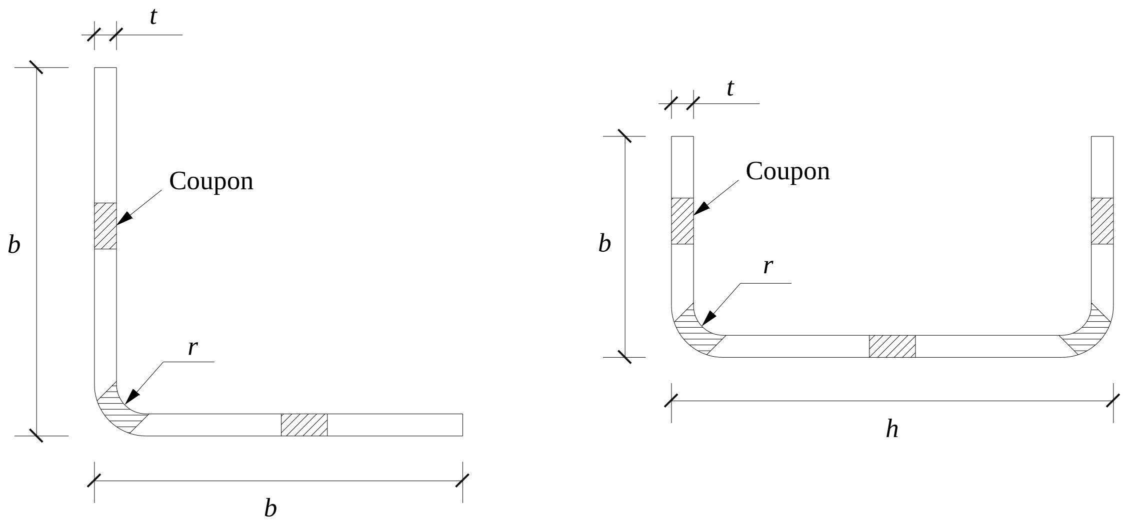

(a) Equal-leg angle section (b) Plain channel section

Fig. 1. Notation and locations of coupons.

Fig. 2. Tensile coupon tests setup.

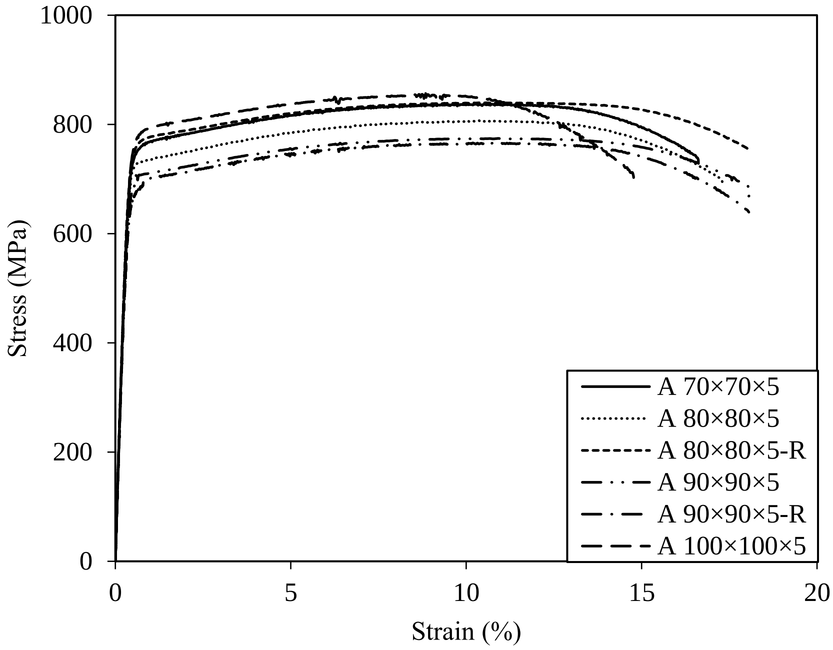

(a) Flat coupons

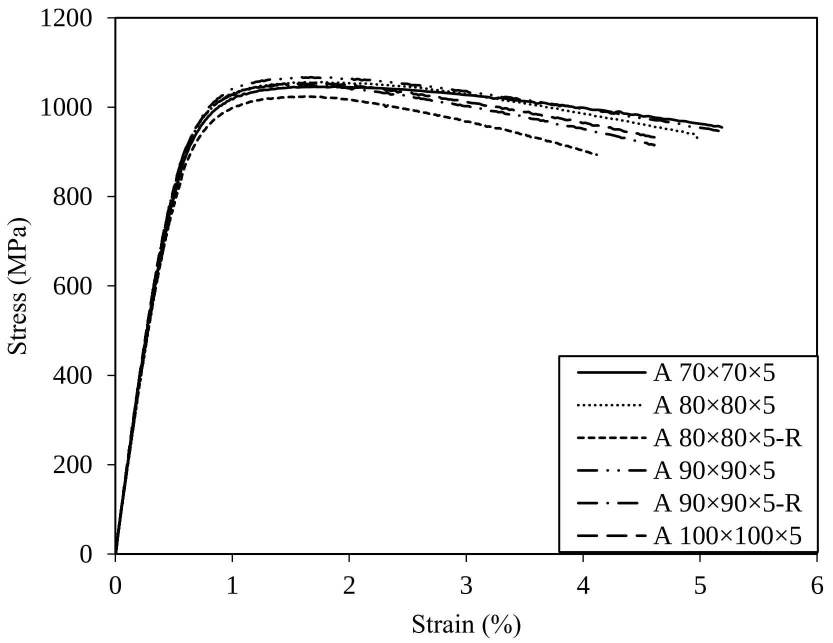

(b) Corner coupons

Fig. 3. Stress–strain curves obtained from material tensile coupon tests on press-braked S690 high strength steel equal-leg angle sections.

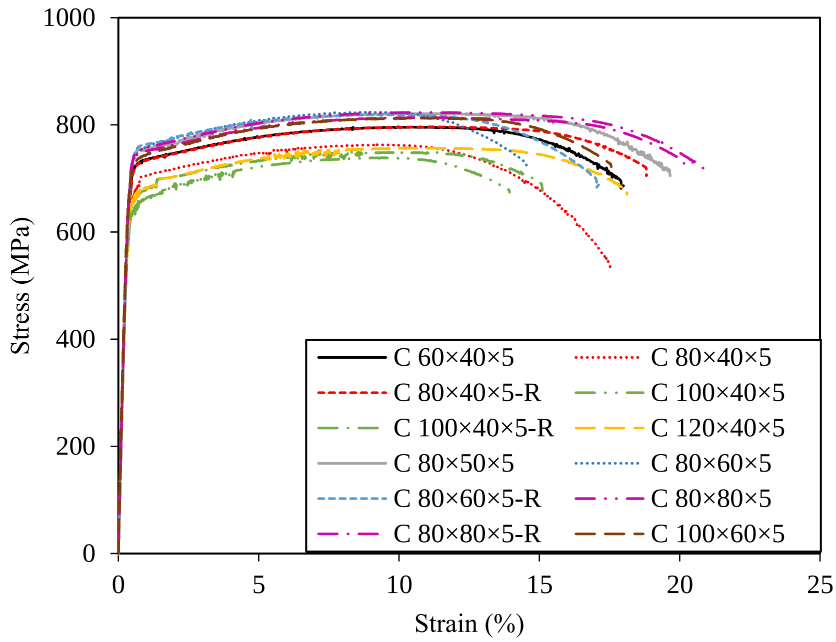

(a) Flat coupons

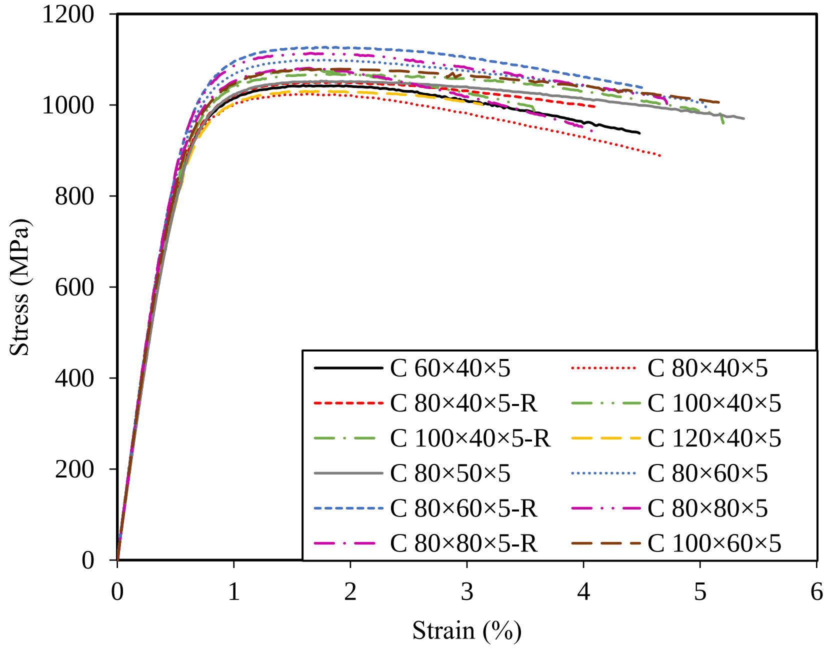

(b) Corner coupons

Fig. 4. Stress–strain curves obtained from material tensile coupon tests on press-braked S690 high strength steel plain channel sections.

(a) Setup for equal-leg angle section specimens

(b) Setup for plain channel section specimens

Fig. 5. Test setups for initial local geometric imperfection measurements.

(a) Setup for equal-leg angle section specimens

(b) Setup for plain channel section specimens

Fig. 6. Stub column test setups.

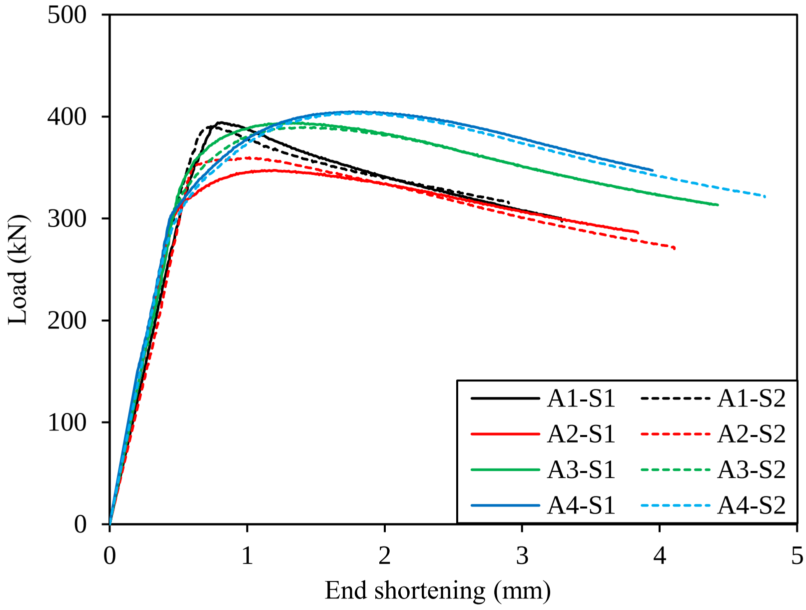

(a) Equal-leg angle section

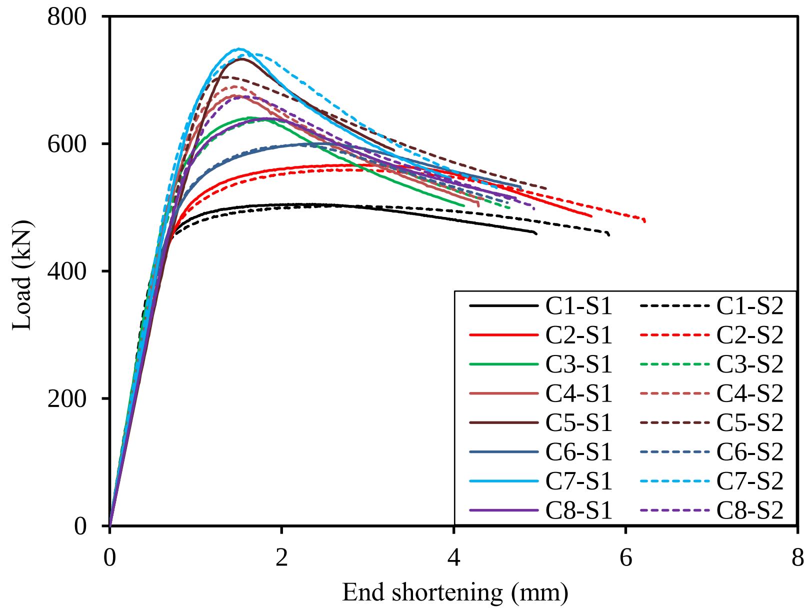

(b) Plain channel section

Fig. 7. Load–end shortening curves of the tested press-braked S690 high strength steel equal-leg angle and plain channel section stub column specimens.

Fig. 8. Failure modes of the tested press-braked S690 high strength steel equal-leg angle and plain channel section stub columns.

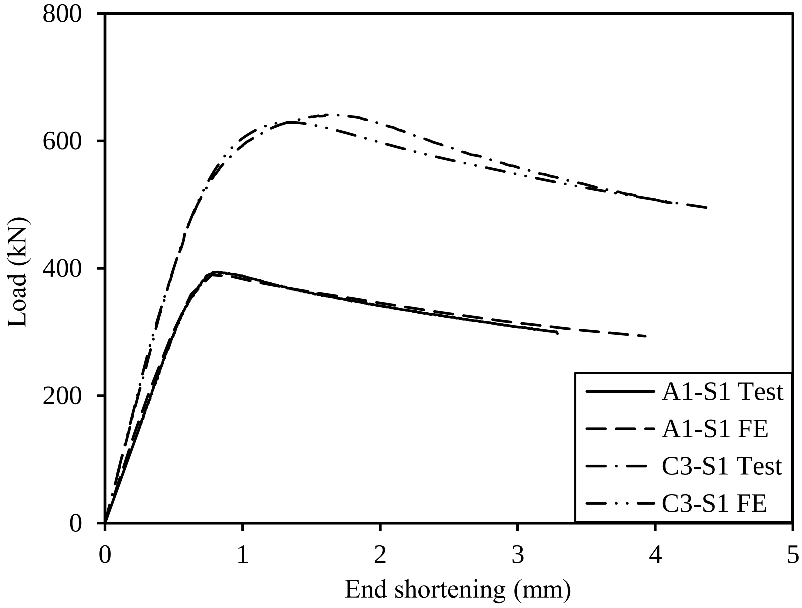

Fig. 9. Experimental and numerical load–end shortening curves for stub column specimens A1-S1 and C3-S1.

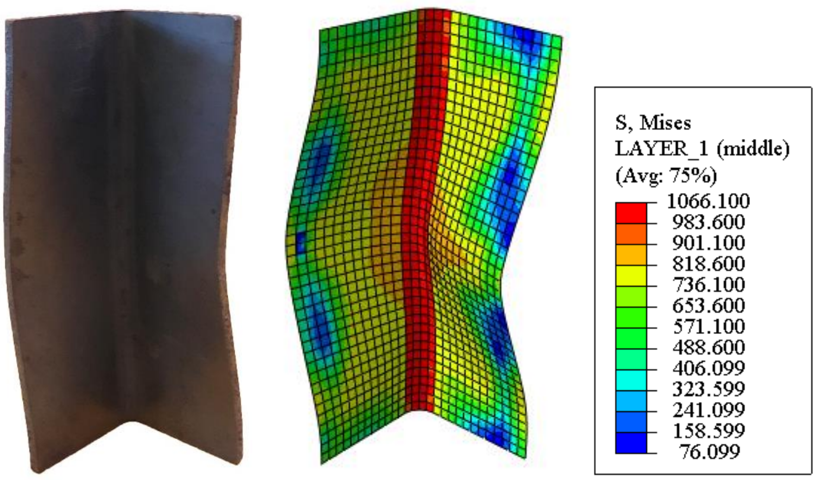

(a) Angle section specimen A1-S1

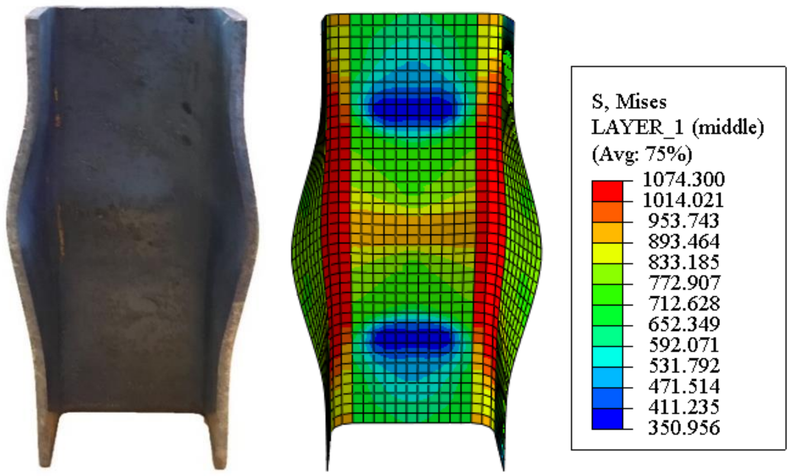

(b) Channel section specimen C3-S1

Fig. 10. Experimental and numerical failure modes for stub column specimens A1-S1 and C3-S1.

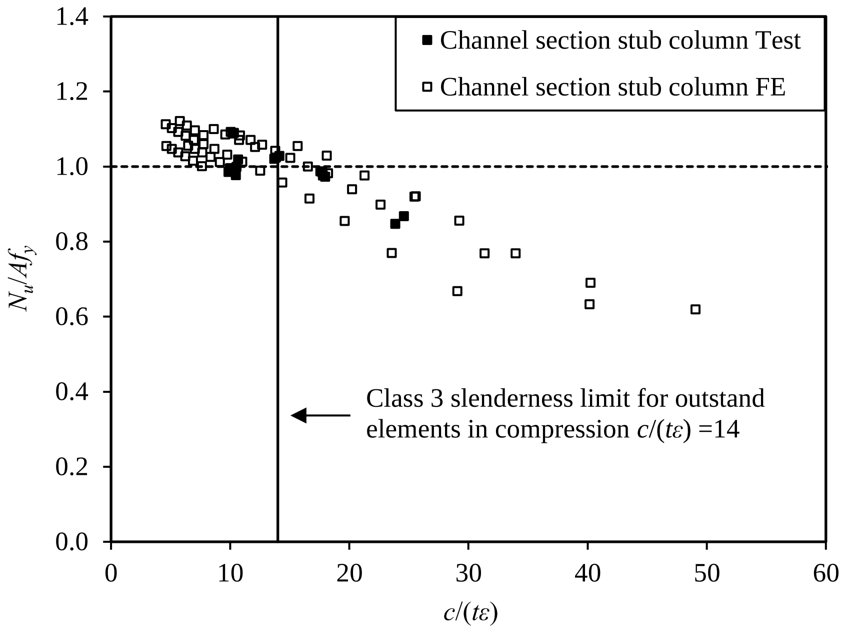

Fig. 11. Assessment of Class 3 slenderness limit for outstand flanges of channel sections in compression.

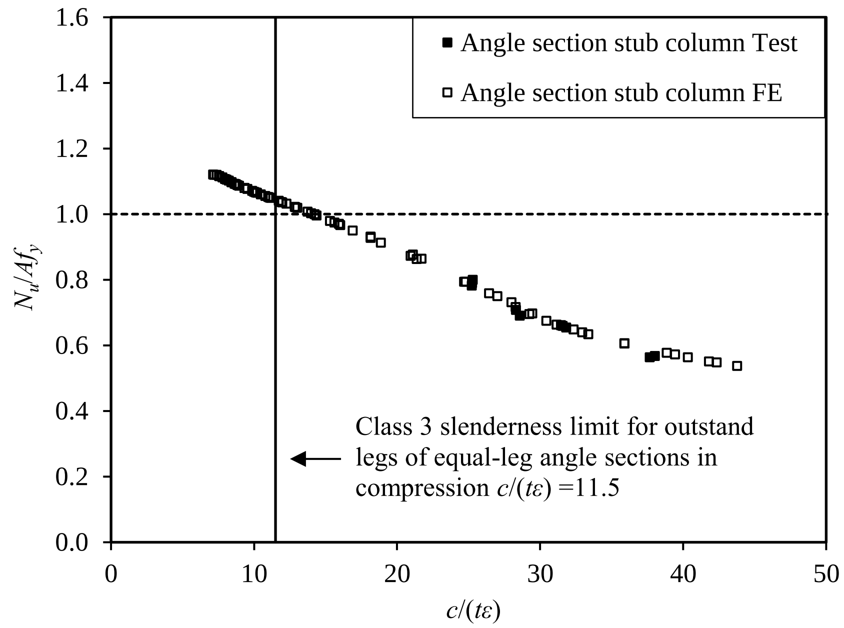

Fig. 12. Assessment of Class 3 slenderness limit for outstand legs of equal-leg angle sections in compression.

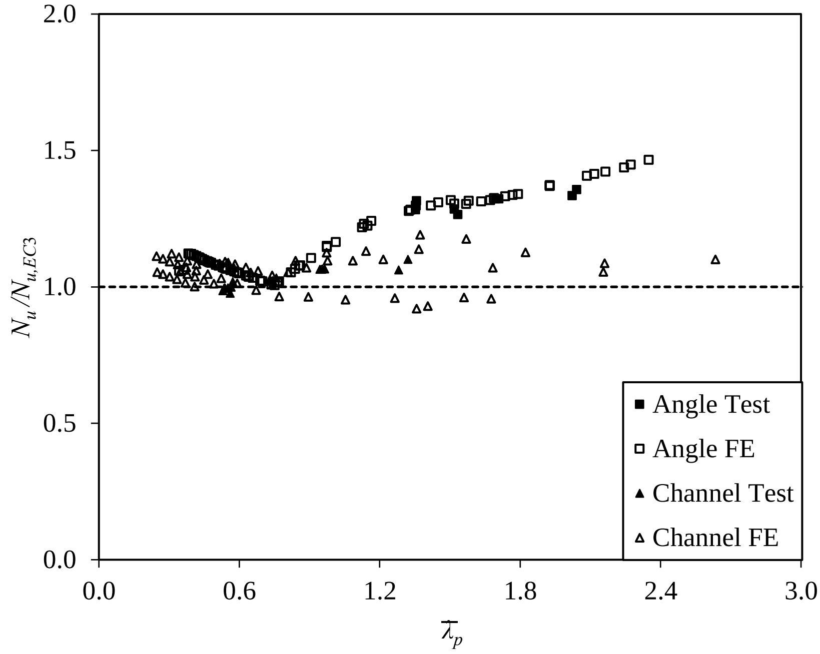

Fig. 13. Comparisons of test and FE results with EN 1993-1-12 strength predictions.

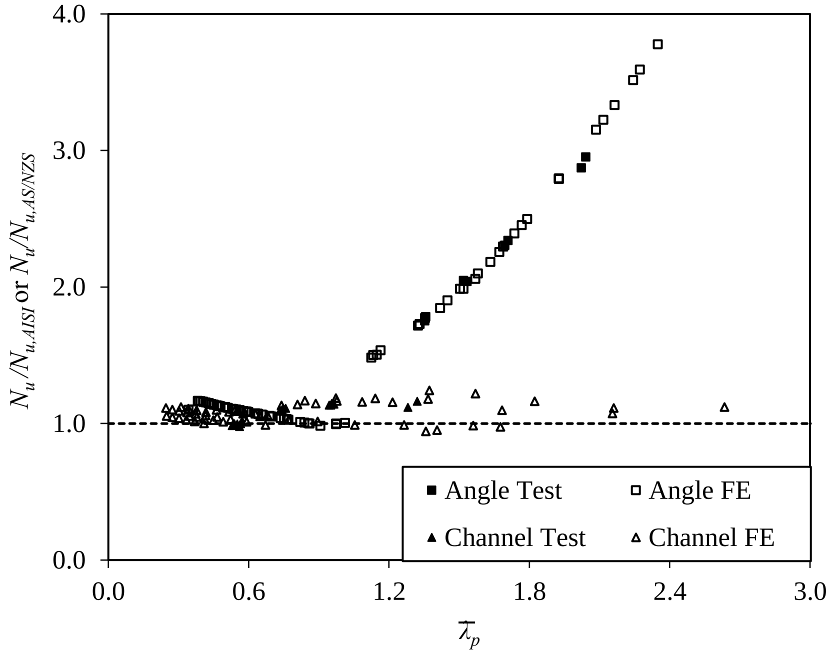

Fig. 14. Comparisons of test and FE results with AISI S100 (and AS/NZS 4600) strength predictions.

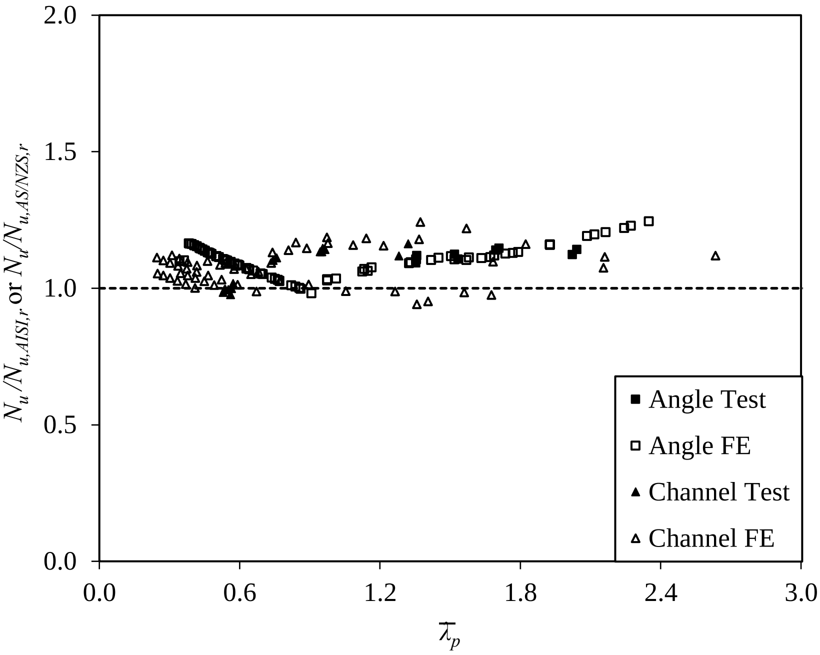

Fig. 15. Comparisons of test and FE results with strength predictions from revised AISI S100 and AS/NZS 4600.

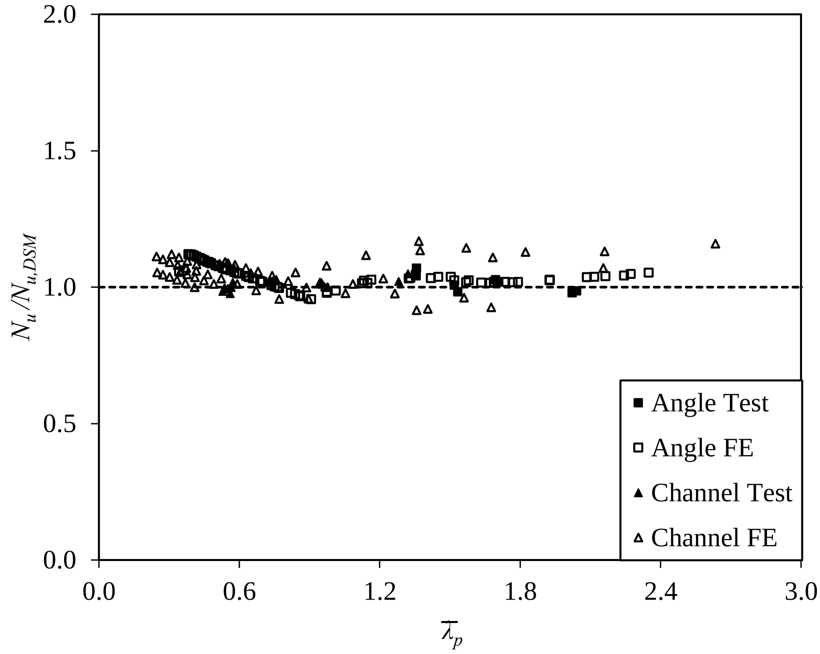

Fig. 16. Comparisons of test and FE results with DSM strength predictions.

Table 1 Summary of key measured material properties from the tensile coupon tests.

(a) Flat coupons

Cross-section	E (GPa)	f_y (MPa)	f_u (MPa)	ε_u (%)	ε_f (%)	f_u/f_y
A 70×70×5	214	741	837	10.3	21.2	1.13
A 80×80×5	213	722	807	10.4	20.0	1.12
A 80×80×5-R	214	752	840	10.6	21.6	1.12
A 90×90×5	209	686	774	10.9	22.8	1.13
A 90×90×5-R	205	667	766	10.2	21.0	1.15
A 100×100×5	213	764	858	8.8	17.0	1.12
C 60×40×5	210	716	796	10.5	22.0	1.11
C 80×40×5	209	663	763	9.2	20.0	1.15
C 80×40×5-R	208	712	796	11.2	22.4	1.12
C 100×40×5	208	635	739	9.4	20.0	1.16
C 100×40×5-R	212	651	752	7.1	20.4	1.16
C 120×40×5	209	658	757	9.9	23.2	1.15
C 80×50×5	210	740	822	11.5	23.2	1.11
C 80×60×5	211	735	825	8.9	19.0	1.12
C 80×60×5-R	209	744	820	9.3	22.2	1.10
C 80×80×5	211	741	823	10.9	25.6	1.11
C 80×80×5-R	212	733	815	10.9	24.6	1.11
C 100×60×5	209	725	813	11.0	22.4	1.12

Note: 'R' indicates a repeated test.

(b) Corner coupons

Cross-section	E (GPa)	f_y (MPa)	σ_u (MPa)	ε_u (%)	ε_f (%)	f_u/f_y
A 70×70×5	191	942	1046	1.7	9.6	1.11
A 80×80×5	194	950	1056	1.6	9.0	1.11
A 80×80×5-R	194	910	1024	1.5	8.4	1.13
A 90×90×5	194	957	1067	1.5	9.2	1.12
A 90×90×5-R	195	955	1051	1.5	8.0	1.10
A 100×100×5	198	949	1054	1.5	8.4	1.11
C 60×40×5	196	932	1043	1.5	9.6	1.12
C 80×40×5	203	920	1025	1.5	8.4	1.11
C 80×40×5-R	193	942	1050	1.7	9.2	1.12
C 100×40×5	194	959	1077	1.5	7.2	1.12
C 100×40×5-R	191	963	1068	1.6	9.0	1.11
C 120×40×5	192	918	1030	1.5	9.0	1.12
C 80×50×5	185	946	1053	1.6	9.6	1.11
C 80×60×5	195	993	1099	1.5	8.0	1.11
C 80×60×5-R	198	1016	1127	1.7	9.0	1.11
C 80×80×5	198	1011	1114	1.6	8.4	1.10
C 80×80×5-R	195	980	1081	1.5	6.4	1.10
C 100×60×5	194	969	1079	1.5	10.0	1.11

Note: 'R' indicates a repeated test.

Table 2
Measured geometric dimensions and initial imperfection for the tested press-braked S690 high strength steel equal-leg angle section stub column specimens.

Specimen ID	b (mm)	t (mm)	r (mm)	L (mm)	ω_{f1} (mm)	ω_{f2} (mm)	ω_0 (mm)	t/ω_0
A1-S1	69.58	4.96	7.44	208.6	0.429	0.408	0.429	11.56
A1-S2	69.92	5.00	7.50	209.6	0.682	0.688	0.688	7.27
A2-S1	79.74	4.80	7.20	239.3	0.665	0.478	0.665	7.22
A2-S2	79.77	4.85	7.28	240.5	0.462	0.198	0.462	10.50
A3-S1	89.74	4.94	7.41	270.1	0.246	0.377	0.377	13.10
A3-S2	89.93	4.91	7.37	270.1	0.563	0.520	0.563	8.72
A4-S1	99.96	4.83	7.25	298.3	0.673	0.639	0.673	7.18
A4-S2	99.86	4.78	7.17	298.0	0.500	0.394	0.500	9.56

Table 3
Measured geometric dimensions and initial imperfection for tested press-braked S690 high strength steel plain channel section stub column specimens.

Specimen ID	b (mm)	h (mm)	t (mm)	r (mm)	L (mm)	ω_{f1} (mm)	ω_{f2} (mm)	ω_w (mm)	ω_0 (mm)	t/ω_0
C1-S1	40.47	59.13	4.94	7.41	149.9	0.334	0.322	0.388	0.388	12.73
C1-S2	40.15	59.28	4.94	7.40	149.2	0.314	0.326	0.314	0.326	15.15
C2-S1	40.68	78.55	4.91	7.37	180.2	0.164	0.234	0.282	0.282	17.41
C2-S2	40.58	78.79	4.94	7.41	176.1	0.316	0.242	0.279	0.316	15.63
C3-S1	50.12	80.16	4.96	7.44	194.5	0.348	0.384	0.308	0.384	12.92
C3-S2	50.39	79.59	4.91	7.37	195.6	0.424	0.382	0.336	0.424	11.58
C4-S1	60.41	80.42	4.88	7.32	209.8	0.482	0.476	0.406	0.482	10.12
C4-S2	60.28	78.77	4.94	7.41	209.5	0.414	0.480	0.404	0.480	10.29
C5-S1	78.84	80.78	4.93	7.39	238.5	0.450	0.428	0.448	0.450	10.96
C5-S2	78.08	79.90	4.97	7.46	240.2	0.400	0.426	0.410	0.426	11.67
C6-S1	39.69	100.40	4.93	7.40	210.5	0.330	0.288	0.188	0.330	14.94
C6-S2	40.38	99.01	4.91	7.37	210.2	0.384	0.132	0.120	0.384	12.79
C7-S1	60.41	99.70	4.93	7.39	239.9	0.268	0.276	0.282	0.282	17.48
C7-S2	60.59	98.66	4.91	7.36	239.4	0.252	0.294	0.262	0.294	16.70
C8-S1	40.33	120.29	4.93	7.40	239.8	0.230	0.344	0.354	0.354	13.93
C8-S2	40.21	120.66	4.97	7.46	239.6	0.330	0.336	0.378	0.378	13.15

Table 4
Summary of stub column test results.

Specimen ID	$N_{u,test}$ (kN)	δ_u (mm)	$N_{u,test}/(Af_y)$	$N_{u,test}/N_{u,EC3}$	$N_{u,test}/N_{u,AISI}$ (or $N_{u,test}/N_{u,AS/NZS}$)	$N_{u,test}/N_{u,AISI,r}$ (or $N_{u,test}/N_{u,AS/NZS,r}$)	$N_{u,test}/N_{u,DSM}$
A1-S1	394.1	0.82	0.80	1.31	1.78	1.12	1.07
A1-S2	390.3	0.74	0.78	1.28	1.75	1.09	1.05
A2-S1	347.3	1.19	0.69	1.26	2.04	1.11	0.98
A2-S2	359.7	1.02	0.71	1.28	2.05	1.12	1.01
A3-S1	393.9	1.40	0.66	1.32	2.31	1.14	1.03
A3-S2	389.5	1.42	0.65	1.32	2.34	1.15	1.02
A4-S1	404.7	1.74	0.56	1.33	2.87	1.12	0.98
A4-S2	403.2	1.76	0.57	1.36	2.95	1.14	0.99
C1-S1	505.2	2.36	1.09	1.09	1.09	1.09	1.09
C1-S2	502.2	2.83	1.09	1.09	1.09	1.09	1.09
C2-S1	566.6	2.95	1.02	1.02	1.02	1.02	1.02
C2-S2	559.3	2.74	1.00	1.00	1.00	1.00	1.00
C3-S1	640.7	1.60	1.02	1.02	1.10	1.10	1.02
C3-S2	637.2	1.82	1.03	1.03	1.11	1.11	1.03
C4-S1	675.8	1.45	0.97	1.07	1.14	1.14	1.00
C4-S2	689.8	1.44	0.98	1.07	1.15	1.15	1.01
C5-S1	732.7	1.73	0.87	1.10	1.16	1.16	1.05
C5-S2	704.4	1.52	0.85	1.06	1.12	1.12	1.02
C6-S1	600.2	2.42	1.00	1.00	1.00	1.00	1.00
C6-S2	598.1	2.11	1.00	1.00	1.00	1.00	1.00
C7-S1	749.0	1.50	0.99	1.06	1.13	1.13	1.02
C7-S2	742.1	1.67	0.98	1.06	1.13	1.13	1.02
C8-S1	639.5	1.79	0.98	0.98	0.98	0.98	0.98
C8-S2	674.1	1.58	0.98	0.98	0.98	0.98	0.98
			Mean	1.13	1.47	1.09	1.02
			COV	0.12	0.43	0.06	0.03

Table 5
Comparison of stub column test failure loads with FE failure loads for varying imperfection amplitudes.

Specimen ID	FE N_u / Test N_u		
	ω_0	$t/10$	$t/100$
A1-S1	1.00	0.99	1.13
A1-S2	0.96	0.99	1.13
A2-S1	1.00	1.02	1.19
A2-S2	1.03	1.02	1.17
A3-S1	1.00	0.99	1.16
A3-S2	0.97	0.97	1.12
A4-S1	1.00	1.05	1.19
A4-S2	1.00	1.00	1.01
C1-S1	0.98	0.97	1.00
C1-S2	0.99	0.98	1.00
C2-S1	0.97	0.95	1.00
C2-S2	0.99	0.97	1.02
C3-S1	0.99	0.98	1.03
C3-S2	0.98	0.98	1.01
C4-S1	0.99	0.99	1.04
C4-S2	0.99	0.99	1.04
C5-S1	1.02	1.01	1.08
C5-S2	1.06	1.05	1.11
C6-S1	0.96	0.94	1.02
C6-S2	0.96	0.95	1.02
C7-S1	0.98	0.96	1.01
C7-S2	0.98	0.96	1.01
C8-S1	0.96	0.94	1.03
C8-S2	0.92	0.90	0.98
Mean	0.99	0.98	1.06
COV	0.03	0.04	0.06

Table 6 Comparisons of test and FE results with predicted strengths.
(a) Press-braked S690 high strength steel equal-leg angle section stub columns

Cross-section type*	No. of test data	No. of FE data	$N_u/N_{u,EC3}$		$N_u/N_{u,AISI}$ (or $N_u/N_{u,AS/NZS}$)		$N_u/N_{u,AISI,r}$ (or $N_u/N_{u,AS/NZS,r}$)		$N_u/N_{u,DSM}$	
			Mean	COV	Mean	COV	Mean	COV	Mean	COV
Non-slender	0	49	1.07	0.03	1.09	0.05	1.09	0.05	1.05	0.05
Slender	8	31	1.32	0.05	1.88	0.58	1.13	0.04	1.02	0.02

* The cross-section type is defined according to EN 1993-1-12 [11].

(b) Press-braked S690 high strength steel plain channel section stub columns

Cross-section type*	No. of test data	No. of FE data	$N_u/N_{u,EC3}$		$N_u/N_{u,AISI}$ (or $N_u/N_{u,AS/NZS}$)		$N_u/N_{u,AISI,r}$ (or $N_u/N_{u,AS/NZS,r}$)		$N_u/N_{u,DSM}$	
			Mean	COV	Mean	COV	Mean	COV	Mean	COV
Non-slender	8	36	1.05	0.04	1.05	0.04	1.05	0.04	1.05	0.04
Slender	8	24	1.06	0.07	1.11	0.07	1.11	0.07	1.04	0.07

* The cross-section type is defined according to EN 1993-1-12 [11].